PNAS RESEARCH ARTICLE | EARTH, ATMOSPHERIC, AND PLANETARY SCIENCES

State shifts in the deep Critical Zone drive landscape evolution in volcanic terrains

Leif Karlstrom[a,1], Nathaniel Klema[b], Gordon E. Grant[c,d], Carol Finn[e], Pamela L. Sullivan[d], Sarah Cooley[f,g], Alex Simpson[a], Becky Fasth[d], Katharine Cashman[a,1], Ken Ferrier[h], Lyndsay Ball[e], and Daniele McKay[a]

Affiliations are included on p. 7.

Contributed by Katharine Cashman; received August 5, 2024; accepted December 2, 2024; reviewed by Louis A. Derry and William E. Dietrich

Volcanic provinces are among the most active but least well understood landscapes on Earth. Here, we show that the central Cascade arc, USA, exhibits systematic spatial covariation of topography and hydrology that are linked to aging volcanic bedrock, suggesting systematic controls on landscape evolution. At the Cascade crest, a locus of Quaternary volcanism, water circulates deeply through the upper ∼1 km of crust but transitions to shallow and dominantly horizontal flow as rocks age away from the arc front. We argue that this spatial pattern reflects a temporal state shift in the deep Critical Zone. Chemical weathering at depth, surface particulate deposition, and tectonic forcing drive landscapes away from an initial state with minimal topographic dissection, large vertical hydraulic conductivity, abundant lakes, and muted hydrographs toward a state of deep fluvial dissection, small vertical hydraulic conductivity, few lakes, and flashy hydrographs. This state shift has major implications for regional water resources. Drill hole temperature profiles imply at least 81 km^3 of active groundwater currently stored at the Cascade Range crest, with discharge variability a strong function of bedrock age. Deeply circulating groundwater also impacts volcanism, and Holocene High Cascades eruptions reflect explosive magma–water interactions that increase regional volcanic hazard potential. We propose that a Critical Zone state shift drives volcanic landscape evolution in wet climates and represents a framework for understanding interconnected solid earth dynamics and climate in these terrains.

Critical Zone | landscape evolution | spring hydrology | volcanism | water resources

Significance

Understanding the near-surface environment where atmospheric and solid earth processes interact, often termed the "Critical Zone," is important for assessing resources and building resilient societies. Here, we examine a volcanic landscape in the Oregon Cascade Range, an understudied Critical Zone setting that is host to major regional water resources, pervasive silicate weathering, and significant geohazards. We leverage a bedrock age chronosequence to show that the volcanic Critical Zone undergoes a structural shift, from depth extents of >1 km to meters, over timescales of ∼1 My. We map an active groundwater volume comparable to major continental lakes, stored at the Cascade Range crest. This state shift makes volcanic landscape evolution a unique probe of deep coupling between Earth systems.

Volcanic terrains showcase Critical Zone (CZ) processes on a grand scale. Among terrestrial landscapes, the CZ is often conceptualized as a weathering "engine" (1), or a permeable near-surface boundary layer where rock, soil, water, air, and living organisms interact (2). Efficient groundwater circulation and meteorically driven chemical weathering extend deeply in young volcanic terrains [commonly >1 km (3)], suggesting a far deeper CZ than the typical tens of meters subsurface extent in many nonvolcanic settings (4). The landscape is volcanically constructed (rather than exhumed through erosion), so initial conditions are knowable in a way that is impossible in most nonvolcanic landscapes, albeit often complex in structure and composition. Time-evolving CZ architecture and sensitivity to environmental perturbations are prominently on display in this setting. Here, we specifically study a CZ "state shift" involving significant, irreversible changes in 1) landscape-scale orientations of groundwater pathways and hydrologic regime, 2) proportion of mass flux due to chemical weathering and dissolved load, and 3) topographic dissection. This state shift provides an exceptional window into CZ evolution, and challenges assumptions about CZ structure.

High rates of topographic construction and physical and chemical erosion make volcanic terrains among the most active on earth. Mafic volcanic landscapes contribute 20 to 35% of modern global CO_2 silicate weathering flux (5, 6) and represent a major source of oceanic silica for diatom production (7), despite occupying ∼6% of current global land area (8). Subsurface fluxes have been inferred to exceed surface chemical erosion (9), and dissolved load is often a dominant contributor to the total fluvial eroded flux (10, 11). Chemical erosion rates tend to decrease with bedrock age, with a ∼10× or more decrease from young (≲0.5 Ma) to older basalts (6, 12). Overall, the reactive nature of volcanic CZ rocks represents a major global carbon cycle feedback (13).

The physical processes driving CZ evolution (e.g., erosion, uplift, hydrology) are also uniquely on display in volcanic landscapes. Volcanic output migrates spatially, repeatedly but incompletely overprinting the landscape and generating dated rock-age sequences that provide powerful space-for-time experiments. Particularly in climatically wet settings,

Author contributions: L.K. designed the study; L.K., G.E.G., N.K., C.F., S.C., A.S., B.F., L.B., and D.M. collected and synthesized data, performed analyses, and made figures; and L.K., N.K., G.E.G., C.F., P.L.S., S.C., K.C., K.F. and L.B. wrote the paper.

Reviewers: L.A.D., Cornell University; and W.E.D., University of California, Berkeley.

The authors declare no competing interest.

[1]To whom correspondence may be addressed. Email: leif@uoregon.edu or cashman@uoregon.edu.

This article contains supporting information online at https://www.pnas.org/lookup/suppl/doi:10.1073/pnas.2415155122/-/DCSupplemental.

Published January 13, 2025.

these terrains are associated with massive aquifers that provide critical water resources but whose hydrologic character and resiliency to change is poorly understood (14, 15). Over half of the large (>1 to 10 m^3/s) springs in the United States occur in volcanic terrains (16). Such springs offer powerful constraints on CZ architecture and dynamics (17).

Time evolution of the CZ is also of interest because it is both influenced by and a control on volcanism. Hydrothermal circulation sets shallow crustal thermal structure and thus the depth and longevity of magma storage (20). Volcanic eruption style is then strongly impacted by near-surface water. Phreatomagmatic eruptions can be highly explosive (21), so a comprehensive understanding of the CZ aids in volcanic hazard assessment.

Here, we demonstrate that surface bedrock ages mirror patterns of topographic dissection, lake occurrence, river and spring hydrology, and groundwater distribution in the central Oregon Cascade Range. To explain this covariation, we hypothesize a CZ state shift, driven by weathering of the volcanic substrate that is modulated by external forcing from climate and tectonics. This hypothesis builds on previously identified contrasts in hydrology and geomorphology (22, 23) with observations of lakes, geophysical imaging of spring architecture, and evidence for magma–water interactions. We argue that this CZ state shift has profound implications for water resources, landscape evolution, and geohazards in volcanic terrains such as the Cascade arc.

A Bedrock Chronosequence. Volcanic output in arc settings is focused toward a narrow, linear band that often migrates perpendicular to the plate boundary over ∼10 Myr timescales (24). In the Cascades, this arc migration is influenced by clockwise tectonic rotation of the Pacific Northwest block relative to the North American plate (25). Central Oregon Quaternary eruption rates of 3 to 6 km^3/Myr/km or more (26) at the arc front repave and inflate the landscape at ∼0.5 mm/y vertically (based on dated volcanic rocks at ∼1 km depths (27), *SI Appendix*). Extensional faulting provides accommodation space within which different timescales of volcanic history can be preserved (25).

As a result, the Oregon Cascades are often described as two adjacent physiographic provinces, the young "High Cascades" and the older "Western Cascades" (28) (Fig. 1*C*). The transition between these provinces reflects what we will argue is a CZ state shift, defined by an east-west gradient of surface bedrock ages (18). We will refer to this age gradient as the Cascades "chronosequence" [acknowledging the ecological definition of this term (29)], permitting study of a CZ hosted within near zero age (eruptions at ∼1 ka) near the topographic crest of the range to >20 Myr age rocks. To the east, a mirror chronosequence also exists, but it is more diffuse and influenced by competing factors discussed later.

Surface age chronosequences have been leveraged in ocean island settings to understand soil, vegetation, hydrology, and topographic evolution (30–32). Despite differences in geometry, glaciation, tectonics, and volcanic output (26, 33, 34), the Cascade arc exhibits similarities to these ocean island chronosequences. Both settings are climatically wet and include a large proportion of mafic volcanism. From a CZ perspective, volcanic deposits exhibit strongly anisotropic hydraulic properties: horizontal permeability dominates at lava flow boundaries and layers of sediment/volcanoclastic fill (35), while vertical permeability dominates in jointed flow interiors (36).

We now outline key datasets that establish the Cascade CZ state shift, from surface to subsurface. We focus on a representative study area centered on the topographic divide of the Oregon Cascades (Fig. 1). The geologic map of Sherrod and Smith (18) constrains surface bedrock ages at sufficient temporal resolution to demonstrate the patterns of interest. To integrate hydrologic data we estimate bedrock ages of gauged streams by weighting their upstream drainage area (*SI Appendix*).

Topography and Surface Water. Meteoric water is delivered via a strong east-west orographic gradient to the Oregon Cascades by snow and rainfall up to ∼2 m/y, with snowpack regulating seasonal hydrologic recharge. The first indicators of a state shift in the CZ are stark topographic differences across the chronosequence. The High Cascades is construction-dominated and relatively undissected, with variably significant glacial erosion. In contrast, the Western Cascades is a fluvially dissected landscape dominated by ridge and valley topography. Because both provinces share similar composition and origin, the development of river networks as the surface ages indicates a CZ state shift. Quantifying drainage density in young volcanic terrain however is challenging because flow routing algorithms do not robustly identify small channels (37). This reflects infiltration-dominated hydrology in primary volcanic rocks that leads to unusual drainage area-discharge relationships (38).

Jefferson et al. (23) proposed that the onset of significant fluvial erosion occurs at 0.5 to 1 Ma, on the basis of increased channel density and drainage-basin averaged bedrock ages. We extend this analysis by computing drainage density as well as local surface slope, comparing to spatially averaged surface ages rather than relying on topographic drainage basins (*SI Appendix*).

In young rocks where fluvial channels are not common but annual precipitation is large, volcanic deposits—modified by Pleistocene montane glaciation (39)—control topography, causing surface water accumulation in lakes. Some of these lakes are seasonally ephemeral (40). We use satellite imagery to map the locations and sizes of 1090 naturally occurring lakes (*SI Appendix*), finding that their distribution overall mirrors bedrock ages <1 Myr (Fig. 1).

Hydrology. Transitions in hydrogeologic structure reflected by emanating spring and stream waters also implicate a state shift in the deep CZ. As water enters the subsurface via rainfall and snowmelt, flow paths defined by burial and infilling of paleosurfaces (35) vary along and across arc. In the High Cascades, several lines of evidence indicate that the hydrogeology is dominated by heterogeneous, permeable structures and vast storage. For example, the extensive depth of hydrothermal circulation relative to aquifer depth in cold springs (36) suggests a nested flow system, where locally recharged compartments are underlain by regionally extensive older waters (41). Regional hydrologic models also imply flowpaths that defy topography (42).

Large discharge springs in the High Cascades typically emerge at the foot of young lava flows or brecciated flow contacts, implying that volcanic units organize groundwater (43). We confirm this with an electrical resistivity tomography (ERT) survey at Olallie North Spring. High resistivity layers (massive core of lava flow lobes and unsaturated, brecciated basalt) are separated by lower resistivity layers associated with saturated, brecciated, and permeable lava flow boundaries where springs appear [(44), Fig. 2 *A* and *B*]. Consistency in the depth of the resistivity transition across the ERT profile and correlation to the spring elevation suggests that groundwater follows the volcanic flow geometry. This site-scale structure confirms inferences from

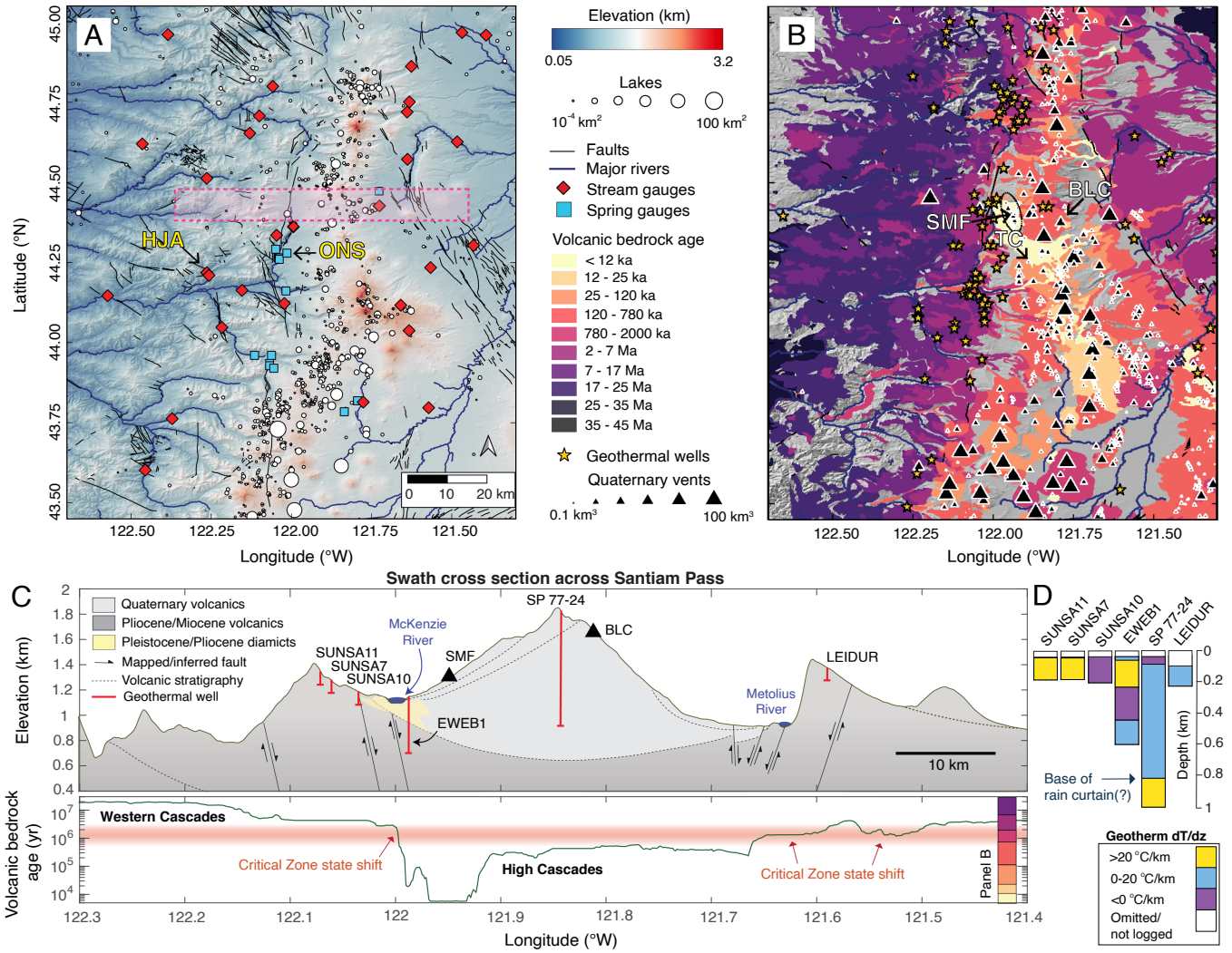

Fig. 1. Oregon Cascades study site. (*A*) Topography, rivers (from USGS blue lines), stream gauges, lakes, and faults. Olallie North Spring (ONS) and HJ Andrews Experimental Forest (HJA) are labeled. (B) Surface bedrock ages (18), geothermal drill holes, and Quaternary volcanic vents (19). Labeled vents exhibited Holocene phreatomagmatic activity: Sand Mountain volcanic field (SMF), Blue Lake Crater (BLC), Twin Craters (TC). Gray areas are mapped as "Sedimentary deposits and rocks" in ref. 18. (*C*) Cross-section of swath topography and surface bedrock ages (N-S average of ±4 km from Santiam Pass, pink box in panel *A*), with subsurface structures based on published geologic maps (*SI Appendix*). The proposed Critical Zone (CZ) state shift and physiographic "Western" and "High" Cascade provinces are labeled. (*D*) Temperature gradient versus depth in drill holes from panel (*C*). Near-isothermal or inverted temperature gradients define the "rain curtain."

regional resistivity models in other volcanic terrains where fluids accumulate and flow laterally within similar structures (45).

Spring discharge varies with seasonal snowpack in a muted, diffusive manner, and this hydrologic behavior dominates the High Cascades (17). In contrast, seasonal storm-driven runoff is significant in older rocks of the Western Cascades (23, 46). We quantify the transition between these end-members via yearly metrics of streams and springs (*SI Appendix*): the range in discharge normalized by mean annual flow, and SD of summer (June–September) discharge normalized by mean annual flow. The former measures hydrograph sensitivity to precipitation events, while the latter characterizes how much summer recession responds to yearly precipitation. Both metrics covary with upstream bedrock age (Fig. 2 *C* and *D* and *SI Appendix*). We classify systems for which annual range in discharge is similar to mean annual discharge as "spring-dominated."

The Rain Curtain. The final indicator of a state shift in the deep CZ is associated with the so-called "rain curtain." Geothermal exploration drilling in the High Cascades encountered unexpected temperature-depth ($T - Z$) profiles that are near isothermal—and in some cases inverted, with temperatures decreasing with depth—in the upper 100 to 1,000 m (Figs. 1*D* and 3*A*). This was attributed to the advection of heat by downward-migrating meteoric water through permeable rocks and was first described at Newberry Volcano (SE of our study area) (47). The depth of the rain curtain likely reflects depths at which heat conduction begins to dominate heat advection by groundwater (48).

Exploration drill holes in our study area (Fig. 1*B*) have shown that the rain curtain is regionally extensive and variably thick (49, 50). Their distribution is spatially biased and drill holes are not always deep enough to resolve rain curtain depth, but in aggregate, they nonetheless constrain regional patterns of groundwater circulation in the deep CZ. For example, Western Cascades rocks exhibit near-linear *T-Z* profiles (51), while High Cascades rocks exhibit 100s m thick near-isothermal sections (Figs. 1*D* and 3*B*). This suggests that the rain curtain shrinks as bedrock ages.

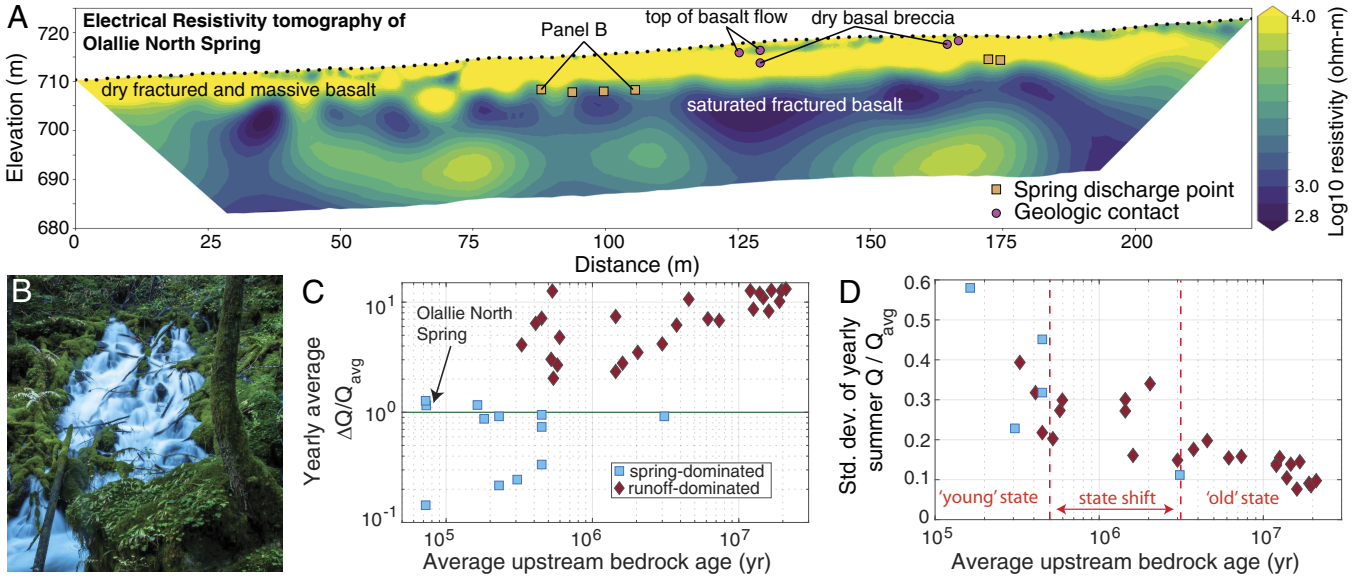

Fig. 2. (*A*) Electrical resistivity tomography of Olallie North Spring, which emerges along a flow contact of ~25 ka Scott Mountain lava flows. Lateral variations correspond to spring discharge points along the lava flow basal breccia such as depicted in (*B*) (photo: Benjamin Nash). (*C*) Mean of total yearly range in discharge ΔQ divided by mean annual flow Q_{avg} versus average upstream age for springs and streams. The horizontal line defines "spring-" versus "runoff-" dominated. (*D*) SD of yearly average summer discharge (June–September), normalized by Q_{avg}, with CZ state shift labeled.

Previous work has also suggested that the rain curtain is absent by the time clay/zeolite alteration (30 to 50 °C) dominates observed weathering mineralogy (52–54). And the depth at which low temperature alteration by groundwater becomes pervasive regionally has been correlated to low electrical resistivity and zeolite-smectite in drill holes (54, 55).

In the Santiam Pass hole SP 77-24, zeolitic alteration of groundmass and within fractures is noted at depths of ~400 m and below ~730 m (27). Drill core porosity fluctuates locally up to 15 to 20% with mean of 6% (Fig. 3*C*), with higher porosity associated with brecciated flow boundaries. Low porosity corresponds to electrically resistive intrusions and massive flows as well as low resistivity clays at the base of the hole (*SI Appendix*). Reactive transport of groundwater in SP 77-24 is further evidenced by oxidation of primary volcanic rocks. Expressed as elevated Fe_2O_3/FeO^* compared to regional Quaternary lavas

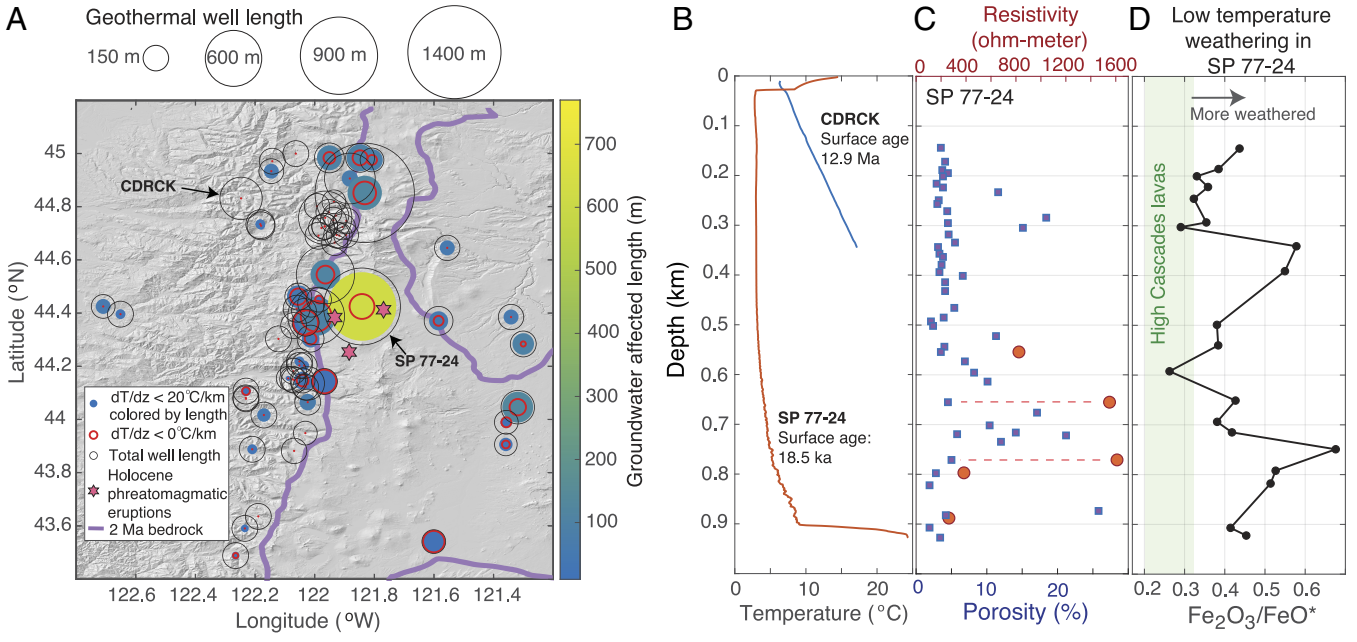

Fig. 3. (*A*) Distribution of geothermal drill holes. Thin black circles' radii scale with total logged length, and colors indicate the fraction of length for which $dT/dz < 20$°C/km (implying downward flux of meteoric water). Red circles are the fraction with inverted gradients ($dT/dz < 0$°C/km). The purple contour indicates bedrock ages <2 Ma, while stars mark Holocene age phreatomagmatic eruption vents. (*B*) Two example temperature-depth logs from deep wells in old and young bedrock. (*C*) Porosity (blue) and resistivity (orange) in the Santiam Pass drill hole SP 77-24. Dashed lines indicate low porosity at high measured resistivity. (*D*) Chemical weathering tracked by oxidation state of iron in the Santiam Pass drill hole. The green box indicates range of Quaternary High Cascades lavas (*SI Appendix*), indicating that much of the SP 77-24 hole has been oxidized.

as proxy for initial concentrations, oxidation peaks at depths where alteration mineralogy is also observed (Fig. 3*D*; additional bulk ratios of mobile to immobile elements are shown in *SI Appendix*). All together, this suggests heterogeneous but pervasive groundwater and low temperature weathering in the High Cascades (54).

We compiled 72 drill hole $T-Z$ profiles in excess of 100 m depth spanning the chronosequence (Fig. 1) to map rain curtain variability. A component of downward groundwater flow parallel to the temperature gradient in rocks will cause bending of otherwise linear $T-Z$ gradients (56), while upwelling/lateral fluid flux can lead to steeper than expected linear gradients (48).

Here, we focus on segments with near isothermal and inverted $T-Z$ profiles which fingerprint downward advection of meteoric water. Previous work has shown that geothermal temperature profiles in our study area can be qualitatively matched with lateral heat advection by groundwater recharging at 0.1 to 1 m/y through a layered aquifer ~1 km thick (22, 57, 58). Groundwater affected ($dT/dz < 20$ °C/km) sections of drill holes shrink with surface bedrock age (*SI Appendix*). The implied aquifer (Fig. 3*A*) maps out a deep and spatially heterogeneous CZ centered on the Quaternary arc front that shallows to the west and east.

Results Summary. East-west surface bedrock age gradients in our study area implicate a CZ state shift that spans topography, surface, and groundwater across the Cascade arc front (Fig. 4). This state shift is spatially diffuse but maps onto a transition away from the physiographic High Cascades province, occurring between ~0.5 to 3 Ma bedrock ages (Fig. 4*B*; see *SI Appendix* for biplots comparing with age directly). It is asymmetric, likely reflecting backarc tectonics and orographic gradients in precipitation/wind that drive erosion and volcanic deposition.

Across the chronosequence, average topographic slope and fluvial channel number density increase with bedrock age (there is no significant age-drainage area correlation, *SI Appendix*). Both metrics imply a shift in the degree to which fluvial erosion shapes topography (23) (Fig. 4*C*). The development of channels and drainage network integration coincides with a decrease of surface water storage in lakes, which mostly occur in <1 Ma age bedrock (Fig. 4*D*) at high elevations.

Hydrologic variability reflects the influence of large but heterogeneous storage in the young CZ. Mean flow of springs hosted in <0.5 Ma bedrock is strongly buffered, with total annual flow range ΔQ similar to the mean Q_{avg} (Figs. 2*C* and 4*E*). For springs hosted in young bedrock, interannual variation in flow during summer recession approaches mean annual flow, while older systems stay within ~10% of the mean (Fig. 2*D*). This points to high throughput and high storage in the High Cascades aquifer. East-west asymmetry in hydrographs (Fig. 4*E*) mirrors the orographic precipitation gradient (Fig. 4*A*).

The depth dimension of the CZ is notoriously challenging to define (4, 59), but the Oregon Cascades provide clear constraints on this cryptic subsurface geometry. Efficient circulation of groundwater is implied by near-isothermal flow pathways associated with the rain curtain underlying young surface bedrock, with depth extent of ~1 km at the Cascade crest that decreases with increasing surface bedrock age (Fig. 4*D*). In the HJ Andrews Experimental Forest (bedrock ages > 7 Ma, Fig. 1), CZ thickness is on the order of meters (60). Exhumation in excess of a kilometer, known through age-constrained stratigraphy (61) (Fig. 1*C*), implies that the fossil record of a thicker weathered CZ has been removed by erosion in the Western Cascades.

Endogenic Forcing of the Critical Zone State Shift. To understand the physical processes responsible for observed state shifts, we first formulate an idealized model for volcanic CZ evolution between end member states. Consider a landscape that is constructed rapidly through volcanism, with negligible erosion and uniform background uplift [perhaps itself magmatic in origin (62)]. The initial surface lacks nonvolcanic relief and an integrated drainage network. From a hydrologic standpoint, fresh volcanic flows are characterized by rubbly, permeable tops, and jointed, denser interiors with large vertical permeability and small horizontal permeability. Volcanic deposits and intrusions compartmentalize groundwater and impart heterogeneous hydraulic properties but high overall storage (*SI Appendix*, Fig. S1*A*).

In time, compaction and alteration/secondary mineral precipitation progressively fill porosity as meteoric water circulates deeply. Surface bedrock breaks down to initiate soil formation, a process accelerated by incipient vegetation (31, 63). Initially thin soil has a high infiltration capacity that does little to alter the dominantly vertical flow paths. Fractured lava flow interiors are affected preferentially by weathering, driving decreases in vertical permeability and integration of groundwater pathways. Advection of deeply sourced volcanic heat (49) increases chemical weathering rates and promotes shallowing of the CZ.

If thickening soil's vertical conductivity becomes sufficiently low [for example through increasing clay content (64)] or alternatively if underlying rock permeability decreases enough, this promotes surface runoff. Fluvial incision initiates, hillslopes steepen, valleys grow, and a hydrologic state shift to runoff-dominated horizontal flow begins (31, 32, 65). This heralds a transition from vertical to lateral water transport overall, and development of a fluvially dissected landscape characterized by paired river channels and hillslopes. After the state shift, hydrologic response time is short and controlled by precipitation events. Fluvial channel incision drives headward valley propagation. Low-gradient remnant surfaces are gradually replaced by steep hillslopes. Low-permeability weathered soils are eroded and replaced with less weathered, higher-permeability soils (66). In the subsurface, high horizontal permeability associated with lava flow boundaries may persist for millions of years (67) (*SI Appendix*, Fig. S1*B*).

Modulation of Critical Zone Evolution by Exogenous Deposition and Faulting. This trajectory for CZ evolution can be modulated by a number of mechanisms at landscape scale. Volcanic inputs of ash and dust can accelerate soil development and evolution (65, 68, 69). For extremely large eruptions, ash deposition smooths topography on 100s km scales (70), and generally imparts hydromechanical anisotropy long after burial. Atmospheric deposition can also impact fluvial processes. For example, particulate deposition accelerated channel incision rates following the 1991 Mt. Pinatubo eruption (71), and fluvial aggradation dramatically increased after the 1980 Mt. Saint Helens eruption (72). In both cases, sediment perturbations persisted for decades. Holocene ash deposition locally in excess of 2 to 3 m has been documented in our study area (73).

Impacts on soil development and fluvial erosion also depend on local composition and rate of exogenous deposition (74, 75). In our study area, a young (1.3 ka) and otherwise undissected lava flow from Collier Cone contains deeply incised channels (38). This has been attributed to glacial-derived fines delivered by debris flows from moraine dam failure, resulting in the development of a low-permeability soil, discontinuous overland flow, and channel incision. Lake occurrence at high elevations in

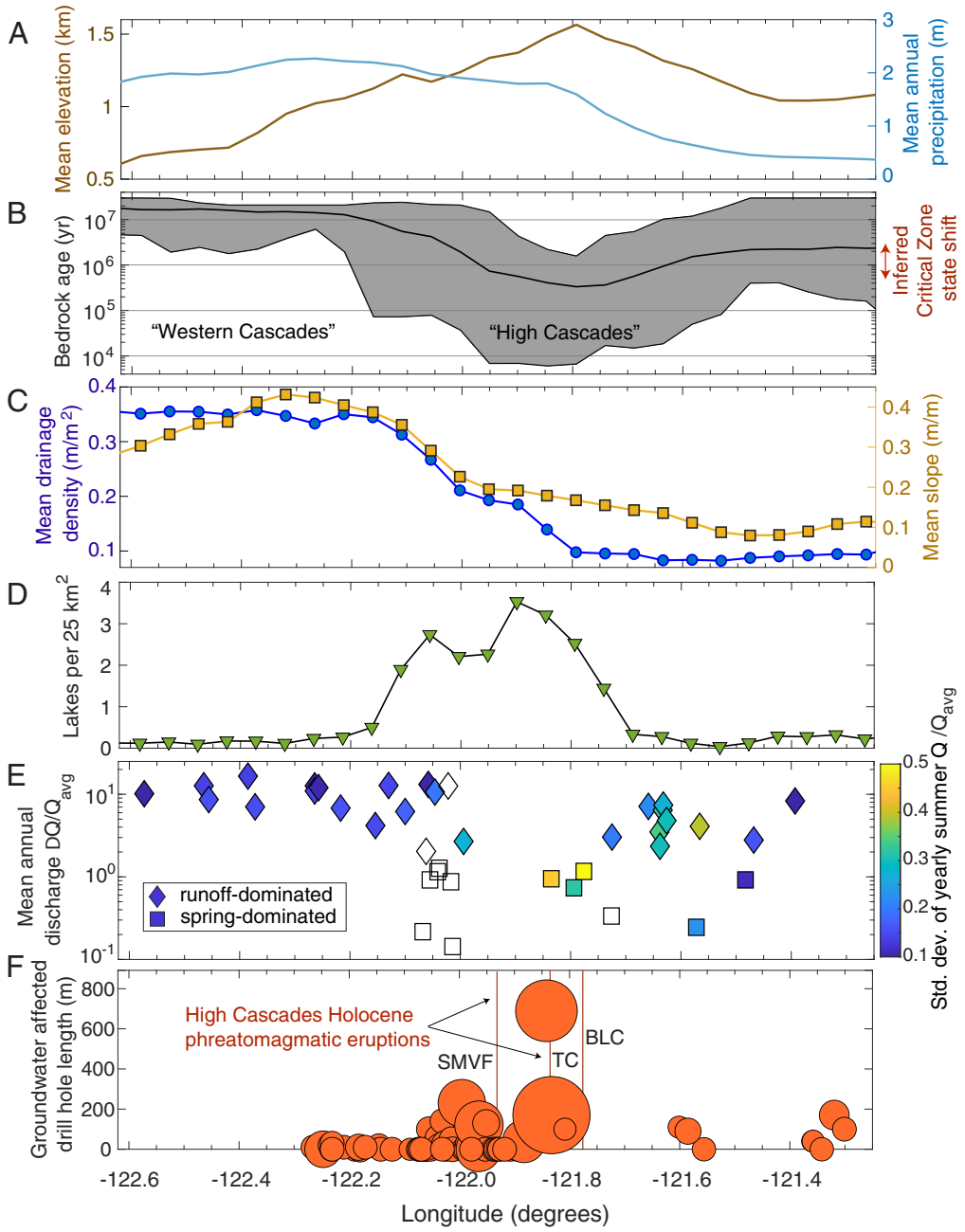

Fig. 4. Variation of CZ state variables with longitude. (*A*) Mean elevations (brown) and mean annual precipitation (blue). (*B*) Surface age (25 km^2 moving average, gray is envelope, black is mean); the red arrow indicates the inferred CZ state shift. (*C*) Topographic dissection, blue is drainage density, and yellow is local slope. (*D*) Surface lake number density. (*E*) Mean annual discharge range ΔQ of springs and streams, colored by SD of annual average June–September flow (open symbols are <3 y records). Both are normalized by annual mean Q_{avg}. (*F*) Near-isothermal (<20 °C/km) sections of drill holes, size of symbol scales with total hole depth. Locations of phreatomagmatic eruptions are vertical lines; see Fig. 1 for names.

our study area (Fig. 4) may also reflect glacially derived sediment, promoting surface water storage in otherwise permeable High Cascades rocks. Zones of exogenous accumulation may be then further influenced and anchored by vegetation, which facilitates accumulation of carbon and organic acids that drive weathering (76).

Finally, tectonic structures and faulting clearly play a role in CZ evolution. Central Cascades volcanism spans a post ~5 Ma extensional graben whose formation predates most of the High Cascades (35). This structure is expressed by discontinuous faults, some of which have offsets of ~1 km, and subsurface stratigraphy (33, 77) (Fig. 1*C*) as well as regional gravity anomalies (78). Extension locally influences aligned volcanic vent locations (33), and faults control the locations of thermal springs (22). In parts of our study site (e.g., Fig. 1*C*), faulting juxtaposes rocks on either side of the state shift, defining the Western and High Cascades physiographic provinces and enhancing exhumation rates to the west. This 100 km scale graben structure defines key initial and boundary conditions for processes driving CZ evolution.

Implications for Volcanic Hazards. A deep CZ impacts the style and thus hazards of Cascades volcanism, because groundwater–magma interactions commonly increase the explosivity of eruptions. Perhaps because of local tectonic extension, central Oregon

eruption rates exceed the Cascades average (26) and showcase these interactions. Despite predominantly mafic magma compositions that typically erupt effusively, a number of recent High Cascades eruptions were explosive and reflect groundwater–magma interaction. The Sand Mountain volcanic field (3 ka), Four in One Cone (2 ka), and Collier Cone (1.5 ka) all erupted explosively, depositing between 0.25 to 3 m of ash over ~10 km^2 (34) (*SI Appendix*). Blue Lake Crater (minimum 1.9 ka) covered 15 km^2 in basaltic tephra (79).

Dramatic explosive phreatomagmatic interactions (seen through tephra textures and particle sorting, *SI Appendix*) occurred in the Sand Mountain volcanic field, erupting near the deepest part of the CZ (Figs. 1*C* and 3*A*). Magma–water interactions could have occurred over at least a kilometer in the final stages of magma ascent. In a thin CZ, the water/magma ratio is smaller and therefore phreatomagmatic eruptions are less likely.

Implications for Landscape Evolution and Water Resources. Volcanic landscapes dominated by basaltic volcanism are a superb yet understudied exemplar of the deep Critical Zone, permitting a unique window into the coevolution of surface and subsurface processes that drive the CZ engine generally. A natural comparison is to karstic landscapes in wet climates, where water also circulates deeply and chemical and physical weathering fronts evolve both from the top down and the bottom up (80). However, whereas limestone enters the weathering zone slowly from below, with porosity and permeability increasing with time, in volcanic landscapes bedrock enters the weathering zone abruptly from the top via eruptions, and from within via intrusions. Permeability generally decreases through time.

The resulting time-dependent bedrock erodibility and fluvial incision patterns (23, 38, 62) represent a challenge for mechanistic geomorphic scaling and transport laws. Sustained magmatic mountain building may involve long-term feedbacks between the solid earth and atmosphere (81) that are poorly understood. And the arc silicate weathering flux is accelerated both by runoff through the volcanic pile (82, 83), and subsurface advection of magmatic heat (84, 85). At Santiam Pass, the rain curtain shoals away from the arc front as surface bedrock ages, implying a thinning rate of ~0.5 to 1 mm/y (*SI Appendix*). This suggests that in the central Cascades, CZ thickness is limited by the ~0.5 mm/y rates of magmatic construction, perhaps analogous to supply-limited behavior exhibited by chemical erosion rates in other landscapes (86). If occlusion of vertical permeability by secondary mineral precipitation (87) shuts off groundwater-dominated heat transport, this likely also sets CZ depth extent and its time-evolution.

For volcanic landscapes in wet climates, large amounts of stored subsurface water represent a critical resource for human populations. The total volume of the High Cascades aquifer and hydrologic response times—key metrics for sensitivity of water resources to perturbations such as climate change—depend on CZ state. Extrapolation of recharge rates or spring discharge over the High Cascades area and multiplication by tritium water ages (mean transit time of 7 to 10 y, acknowledging that longer transit times are also likely involved depending on flow path) gives a volume of ~35 km^3 (43). We interpolate (via kriging, *SI Appendix*) near-isothermal sections of drill holes below 30 m depths to estimate the volume of crust that hosts downward advection of meteoric water. Assuming 6% average porosity (27) (Fig. 3*C*), the active groundwater volume is ~81 km^3. This is a lower bound (*SI Appendix*), because drill holes do not map the full rain curtain extent, and we do not attempt to account for upflow.

The significance of this aquifer is equally apparent by considering fluxes: Groundwater flux based on springs is ~1 km^3/y, whereas that inferred from regional water balance is ~11 km^3/y (*SI Appendix*). This segment of the High Cascades is therefore similar to the Hawaiian Islands in total groundwater flux (88), and we note that other large Cascade aquifers near Mt. Adams and Lassen/Medicine Lake are also hosted in mafic Quaternary rocks (89). Given increased human pressure on aquifer resources and decreasing snowpack in a warming climate (90), the fact that springs in the young CZ are proportionally more responsive to interannual climate variability (Fig. 2*D*) than those in the old CZ implies a need for better characterization of these systems.

Metrics of CZ state identified here frame the competition between magma and water that shapes volcanic landscapes over time. Although they may take a different form elsewhere, we expect that landscape-scale state shifts such as seen in the Cascade arc are common. The legacy of transitions associated with coupling between earth systems, rather than steady-state conditions (91), may provide a useful framework for probing the structure and evolution of these landscapes.

Data, Materials, and Software Availability. Time not available elsewhere series data have been deposited in hydroshare (92), and US Geological Survey data release (93). Previously published data were used for this work (references in manuscript and supplement).

ACKNOWLEDGMENTS. We were supported by the following NSF awards during this project: 1848554 to L.K. and 2121694 and 2012796 to P.L.S. G.E.G. acknowledges support from US Department of Agriculture Forest Service, Pacific Northwest Research Station. We acknowledge discussions with Richard Conrey, Anne Jefferson, Kate Maher, and David Sherrod throughout the development of this work. Our interpretations rely on seminal field studies in this area by David Sherrod, Ed Taylor, and Anne Jefferson. The cross-section in Fig. 1*C* is inspired by David Sherrod. Steve Ingebritsen supplied binders containing geothermal drill hole logs that were digitized to supplement published databases. Thorough and constructive reviews were provided by William Dietrich, Louis Derry, and Steve Ingebritsen.

Author affiliations: [a]Department of Earth Sciences, University of Oregon, Eugene, OR 97403; [b]Department of Physics and Engineering, Fort Lewis College, Durango, CO 81301; [c]Pacific Northwest Research Station, United States Forest Service, Corvallis, OR 87331; [d]College of Earth, Ocean, and Atmospheric Sciences, Oregon State University, Corvallis, OR 97331; [e]Geology, Geophysics, Geochemistry Science Center, United States Geological Survey, Denver, CO 80225; [f]Nicholas School of the Environment, Duke University, Durham, NC 27302; [g]Department of Geography, University of Oregon, Eugene, OR 97403; and [h]Department of Geoscience, University of Wisconsin, Madison, WI 53706

1. S. P. Anderson *et al*., Proposed initiative would study Earth's weathering engine. *EOS Trans. Am. Geophys. Union* **85**, 265–269 (2004).
2. National Research Council, *Basic Research Opportunities in Earth Science* (The National Academies Press, Washington, DC, 2001).
3. G. Büttner, E. Huenges, The heat transfer in the region of the Mauna Kea (Hawaii)-constraints from borehole temperature measurements and coupled thermo-hydraulic modeling. *Tectonophysics* **371**, 23–40 (2003).
4. C. S. Riebe, W. J. Hahm, S. L. Brantley, Controls on deep critical zone architecture: A historical review and four testable hypotheses. *Earth Surf. Proc. Land.* **42**, 128–156 (2017).
5. C. Dessert, B. Dupré, J. Gaillardet, L. M. François, C. J. Allègre, Basalt weathering laws and the impact of basalt weathering on the global carbon cycle. *Chem. Geol.* **202**, 257–273 (2003).
6. J. Börker, J. Hartmann, G. Romero-Mujalli, G. Li, Aging of basalt volcanic systems and decreasing CO_2 consumption by weathering. *Earth Surf. Dyn.* **7**, 191–197 (2019).
7. P. J. Tréguer, C. L. De La Rocha, The world ocean silica cycle. *Ann. Rev. Mar. Sci.* **5**, 477–501 (2013).
8. J. Hartmann, N. Moosdorf, The new global lithological map database GLiM: A representation of rock properties at the Earth surface. *Geochem. Geophys. Geosyst.* **13**, Q12004 (2012).
9. H. H. Schopka, L. A. Derry, Chemical weathering fluxes from volcanic islands and the importance of groundwater: The Hawaiian example. *Earth Planet. Sci. Lett.* **339**, 67–78 (2012).
10. J. E. O'Connor, J. F. Mangano, D. R. Wise, J. R. Roering, Eroding Cascadia-Sediment and solute transport and landscape denudation in western Oregon and Northwestern California. *GSA Bull.* **133**, 1851–1874 (2021).

11. T. L. Cole, M. A. Torres, P. C. Kemeny, The hydrochemical signature of incongruent weathering in Iceland. *J. Geophys. Res. Earth Surf.* **127**, e2021JF006450 (2022).
12. S. Rad, K. Rivé, B. Vittecoq, O. Cerdan, C. J. Allègre, Chemical weathering and erosion rates in the Lesser Antilles: An overview in Guadeloupe, Martinique and Dominica. *J. S. Am. Earth Sci.* **45**, 331–344 (2013).
13. S. Brantley, A. Shaughnessy, M. I. Lebedeva, V. N. Balashov, How temperature-dependent silicate weathering acts as Earth's geological thermostat. *Science* **379**, 382–389 (2023).
14. K. A. Farley, C. Tague, G. E. Grant, Vulnerability of water supply from the Oregon Cascades to changing climate: Linking science to users and policy. *Glob. Environ. Chang.* **21**, 110–122 (2011).
15. M. S. Waibel, M. W. Gannett, H. Chang, C. L. Hulbe, Spatial variability of the response to climate change in regional groundwater systems-Examples from simulations in the Deschutes Basin, Oregon. *J. Hydrol.* **486**, 187–201 (2013).
16. O. E. Meinzer, "Large springs in the United States" (No. 557, US Government Printing Office, 1927).
17. M. Manga, On the timescales characterizing groundwater discharge at springs. *J. Hydrol.* **219**, 56–69 (1999).
18. D. R. Sherrod, J. G. Smith, *Geologic Map of Upper Eocene to Holocene Volcanic and Related Rocks of the Cascade Range, Oregon* (US Geological Survey Washington, DC, 2000).
19. D. O'Hara, L. Karlstrom, D. W. Ramsey, Time-evolving surface and subsurface signatures of Quaternary volcanism in the Cascades arc. *Geology* **48**, 1088–1093 (2020).
20. J. Eichelberger, Distribution and transport of thermal energy within magma-hydrothermal systems. *Geosciences* **10**, 212 (2020).
21. B. Zimanowski, R. Büttner, P. Dellino, J. D. White, K. H. Wohletz, "Magma-water interaction and phreatomagmatic fragmentation" in *The encyclopedia of volcanoes*, H. Sigurdsson, B. Houghton, H. Rymer, J. Stix, S. McNutt, Eds. (Elsevier, 2015), pp. 473–484.
22. S. E. Ingebritsen, R. H. Mariner, D. R. Sherrod, "Hydrothermal systems of the Cascade Range, north-central Oregon" (No. 1044-L, US Government Printing Office, 1994).
23. A. Jefferson, G. Grant, S. Lewis, S. Lancaster, Coevolution of hydrology and topography on a basalt landscape in the Oregon Cascade Range, USA. *Earth Surf. Proc. Land. J. Br. Geomorphol. Res. Group* **35**, 803–816 (2010).
24. L. Karlstrom, C. T. Lee, M. Manga, The role of magmatically driven lithospheric thickening on arc front migration. *Geochem. Geophys. Geosyst.* **15**, 2655–2675 (2014).
25. R. E. Wells, R. McCaffrey, Steady rotation of the Cascade arc. *Geology* **41**, 1027–1030 (2013).
26. D. R. Sherrod, J. G. Smith, Quaternary extrusion rates of the Cascade Range, Northwestern United States and Southern British Columbia. *J. Geophys. Res. Solid Earth* **95**, 19465–19474 (1990).
27. B. E. Hill, "Geology and geothermal resources of the Santiam Pass area of the Oregon Cascade Range, Deschutes, Jefferson and Linn Counties, Oregon" (No. DOE/ID/12834-13; USGS-OFR-0-92-3, Oregon State Dept. of Geology and Mineral Industries, Portland, OR, 1992).
28. E. Callaghan, Some features of the volcanic sequence in the Cascade Range in Oregon. *EOS Trans. Am. Geophys. Union* **14**, 243–249 (1933).
29. L. R. Walker, D. A. Wardle, R. D. Bardgett, B. D. Clarkson, The use of chronosequences in studies of ecological succession and soil development. *J. Ecol.* **98**, 725–736 (2010).
30. O. A. Chadwick, L. A. Derry, P. M. Vitousek, B. J. Huebert, L. O. Hedin, Changing sources of nutrients during four million years of ecosystem development. *Nature* **397**, 491–497 (1999).
31. K. A. Lohse, W. E. Dietrich, Contrasting effects of soil development on hydrological properties and flow paths. *Water Resour. Res.* **41**, W12419 (2005).
32. A. Perez-Fodich, L. A. Derry, J. Marçais, M. T. Walter, The effect of weathering in runoff-to-groundwater partitioning in the Island of Hawai'i: Perspectives for landscape evolution. *Earth Planet. Sci. Lett.* **635**, 118687 (2024).
33. R. M. Conrey, E. M. Taylor, J. M. Donnelly-Nolan, D. R. Sherrod, G. Moore, North-central Oregon Cascades: Exploring petrologic and tectonic intimacy in a propagating intra-arc rift. *Field Guide Geol. Process. Cascadia* **36**, 47–90 (2002).
34. N. I. Deligne *et al*., "Field-trip guide to mafic volcanism of the Cascade Range in Central Oregon–A volcanic, tectonic, hydrologic, and geomorphic journey" (No. 2017-5022-H, US Geological Survey, 2017).
35. E. M. Taylor, Volcanic history and tectonic development of the central High Cascade Range, Oregon. *J. Geophys. Res. Solid Earth* **95**, 19611–19622 (1990).
36. M. Manga, Advective heat transport by low-temperature discharge in the Oregon Cascades. *Geology* **26**, 799–802 (1998).
37. W. Luo, T. Stepinski, Identification of geologic contrasts from landscape dissection pattern: An application to the Cascade Range, Oregon, USA. *Geomorphology* **99**, 90–98 (2008).
38. K. E. Sweeney, J. J. Roering, Rapid fluvial incision of a late Holocene lava flow: Insights from LiDAR, alluvial stratigraphy, and numerical modeling. *Bulletin* **129**, 500–512 (2017).
39. J. J. Morley, B. A. Dworetzky, Evolving Pliocene-Pleistocene climate: A north Pacific perspective. *Quatern. Sci. Rev.* **10**, 225–237 (1991).
40. F. C. Ziesenhenne, *Lake Survey of the Willamette National Forest* (US Forest Service, 1936).
41. C. Roques *et al*., Recession discharge from compartmentalized bedrock hillslopes. *Hydrol. Earth Syst. Sci. Discuss.* **2022**, 1–24 (2022).
42. M. W. Gannett, K. E. Lite Jr., J. C. Risley, E. M. Pischel, J. L. La Marche, "Simulation of groundwater and surface-water flow in the upper Deschutes Basin, Oregon" (No. 2017-5097, US Geological Survey, 2017).
43. A. Jefferson, G. Grant, T. Rose, Influence of volcanic history on groundwater patterns on the west slope of the Oregon High Cascades. *Water Resour. Res.* **42**, W12411 (2006).
44. H. T. Stearns, "Geology and water resources of the Upper McKenzie Valley, Oregon" (No. 597-D, US Government Printing Office, 1929).
45. C. A. Finn *et al*., Geophysical imaging of the Yellowstone hydrothermal plumbing system. *Nature* **603**, 643–647 (2022).
46. C. Tague, G. E. Grant, A geological framework for interpreting the low-flow regimes of Cascade streams, Willamette River Basin, Oregon. *Water Resour. Res.* **40**, W04303 (2004).
47. C. A. Swanberg, W. C. Walkey, J. Combs, Core hole drilling and the "rain curtain" phenomenon at Newberry Volcano, Oregon. *J. Geophys. Res. Solid Earth* **93**, 10163–10173 (1988).
48. M. O. Saar, Geothermal heat as a tracer of large-scale groundwater flow and as a means to determine permeability fields. *Hydrogeol. J.* **19**, 31 (2011).
49. S. Ingebritsen, D. Sherrod, R. H. Mariner, Heat flow and hydrothermal circulation in the Cascade Range, north-central Oregon. *Science* **243**, 1458–1462 (1989).
50. D. D. Blackwell *et al*., Heat flow in the Oregon Cascade Range and its correlation with regional gravity, Curie point depths, and geology. *J. Geophys. Res. Solid Earth* **95**, 19475–19493 (1990).
51. S. Ingebritsen, M. Scholl, D. Sherrod, Heat flow from four new research drill holes in the Western Cascades, Oregon, USA. *Geothermics* **22**, 151–163 (1993).
52. W. Youngquist, "Geothermal gradient drilling, north-central Cascades of Oregon, 1979" (No. DOE/ET/27243-T1, Oregon State Dept. of Geology and Mineral Industries, Portland, USA, 1980).
53. D. D. Blackwell, S. A. Kelley, J. L. Steele, "Heat flow modeling of the Snake River Plain, Idaho" (U.S. Dept. of Energy Contract DE-AC07-761DO1570, Dept. of Geological Sciences, Southern Methodist Univ., 1992), 109 pp.
54. G. L. Black, *Geothermal Electrical Power Generation Potential of Newberry Volcano and the Oregon Cascade Range* (State of Oregon, Department of Geology and Mineral Industries, No. 0-7, 1994).
55. T. Keith, "Regional patterns of hydrothermal alteration in the Breitenbush-Austin hot springs area of the Cascade range, Oregon" in *Geology and Geothermal Resources of the Breitenbush-Austin Hot Springs Area, Clackamas and Marion Counties, Oregon: Oregon Department of Geology and Mineral Industries Open-File Report O-88-5* (Geothermal Resources Council, 1988), pp. 31–37.
56. J. D. Bredehoeft, I. Papaopulos, Rates of vertical groundwater movement estimated from the Earth's thermal profile. *Water Resour. Res.* **1**, 325–328 (1965).
57. S. Ingebritsen, D. Sherrod, R. Mariner, Rates and patterns of groundwater flow in the Cascade Range volcanic arc, and the effect on subsurface temperatures. *J. Geophys. Res. Solid Earth* **97**, 4599–4627 (1992).
58. M. O. Saar, M. Manga, Depth dependence of permeability in the Oregon Cascades inferred from hydrogeologic, thermal, seismic, and magmatic modeling constraints. *J. Geophys. Res. Solid Earth* **109**, B04204 (2004).
59. L. E. Condon *et al*., Where is the bottom of a watershed?. *Water Resour. Res.* **56**, e2019WR026010 (2020).
60. R. Harmon, H. R. Barnard, K. Singha, Water table depth and bedrock permeability control magnitude and timing of transpiration-induced diel fluctuations in groundwater. *Water Resour. Res.* **56**, e2019WR025967 (2020).
61. D. R. Sherrod, *Geology and geothermal resources of the Breitenbush-Austin Hot Springs area, Clackamas and Marion Counties, Oregon* (State of Oregon, Department of Geology and Mineral Industries, 1988).
62. N. Klema *et al*., The magmatic origin of the Columbia River Gorge, USA. *Sci. Adv.* **9**, eadj3357 (2023).
63. S. Porder, G. E. Hilley, O. A. Chadwick, Chemical weathering, mass loss, and dust inputs across a climate by time matrix in the Hawaiian Islands. *Earth Planet. Sci. Lett.* **258**, 414–427 (2007).
64. I. N. Candra *et al*., Soil development and mineral transformations along a one-million-year chronosequence on the Galápagos Islands. *Soil Sci. Soc. Am. J.* **85**, 2077–2099 (2021).
65. P. Vitousek *et al*., Erosion and the rejuvenation of weathering-derived nutrient supply in an old tropical landscape. *Ecosystems* **6**, 762–772 (2003).
66. A. M. Heimsath, W. E. Dietrich, K. Nishiizumi, R. C. Finkel, The soil production function and landscape equilibrium. *Nature* **388**, 358–361 (1997).
67. T. L. Tolan *et al*., "Stratigraphy and tectonics of the central and eastern portions of the Columbia River Flood-Basalt Province: An overview of our current state of knowledge" in *Volcanoes to Vineyards: Geologic Field Trips through the Dynamic Landscape of the Pacific Northwest*, J. E. O'Connor, R. J. Dorsey, I. P. Madin, Eds. (Geological Society of America, 2009).
68. S. G. Wells, J. C. Dohrenwend, L. D. McFadden, B. D. Turrin, K. D. Mahrer, Late Cenozoic landscape evolution on lava flow surfaces of the Cima Volcanic field, Mojave Desert, California. *Geol. Soc. Am. Bull.* **96**, 1518–1529 (1985).
69. M. Eppes, J. Harrison, Spatial variability of soils developing on basalt flows in the Potrillo volcanic field, southern New Mexico: Prelude to a chronosequence study. *Earth Surf. Proc. Land.* **24**, 1009–1024 (1999).
70. V. Manville, C. J. Wilson, The 26.5 ka Oruanui eruption, New Zealand: A review of the roles of volcanism and climate in the post-eruptive sedimentary response. *N. Z. J. Geol. Geophys.* **47**, 525–547 (2004).
71. D. R. Montgomery, M. S. Panfil, S. K. Hayes, Channel-bed mobility response to extreme sediment loading at Mount Pinatubo. *Geology* **27**, 271–274 (1999).
72. J. J. Major, T. Pierson, R. Dinehart, J. Costa, Sediment yield following severe volcanic disturbance-a two-decade perspective from Mount St. Helens. *Geology* **28**, 819–822 (2000).
73. D. McKay, "Recent mafic eruptions at Newberry Volcano and in the central Oregon Cascades: Physical volcanology and implications for hazards," doctoral dissertation, University of Oregon, Eugene, OR (2012).
74. G. H. Brimhall *et al*., Metal enrichment in bauxites by deposition of chemically mature aeolian dust. *Nature* **333**, 819–824 (1988).
75. S. M. Aciego *et al*., Dust outpaces bedrock in nutrient supply to montane forest ecosystems. *Nat. Commun.* **8**, 14800 (2017).
76. N. I. Deligne, K. V. Cashman, J. J. Roering, After the lava flow: The importance of external soil sources for plant colonization of recent lava flows in the central Oregon Cascades, USA. *Geomorphology* **202**, 15–32 (2013).
77. D. R. Sherrod, L. G. Pickthorn, "Some notes on the Neogene structural evolution of the Cascade Range in Oregon" in *Geological, Geophysical, and Tectonic Setting of the Cascade Range*, L. J. P. Muffler, C. S. Weaver, D. D. Blackwell, Eds. (US Geological Survey Open File Report 89-178, 1989), pp. 351–368.
78. R. W. Couch, G. S. Pitts, M. Gemperle, D. E. Braman, C. A. Veen, "Gravity anomalies in the Cascade Range in Oregon –Structural and thermal implications" (Oregon Department of Geology and Mineral Industries Open-File Report O-82-9, 1982), 66 p.
79. E. R. Johnson, K. V. Cashman, Understanding the storage conditions and fluctuating eruption style of a young monogenetic volcano: Blue Lake crater (<3 ka), High Cascades, Oregon. *J. Volcanol. Geotherm. Res.* **408**, 107103 (2020).
80. P. Sullivan, G. Macpherson, J. Martin, R. Price, Evolution of carbonate and karst critical zones. *Chem. Geol.* **527**, 119223 (2019).
81. D. O'Hara, L. Karlstrom, The arc-scale spatial distribution of volcano erosion implies coupled magmatism and regional climate in the Cascades arc, United States. *Front. Earth Sci.* **11**, 1150760 (2023).

82. S. R. Gislason, S. Arnórsson, H. Ármannsson, Chemical weathering of basalt in southwest Iceland; Effects of runoff, age of rocks and vegetative/glacial cover. *Am. J. Sci.* **296**, 837–907 (1996).
83. J. Gaillardet *et al*., Orography-driven chemical denudation in the Lesser Antilles: Evidence for a new feed-back mechanism stabilizing atmospheric CO_2. *Am. J. Sci.* **311**, 851–894 (2011).
84. A. Aiuppa *et al*., Mobility and fluxes of major, minor and trace metals during basalt weathering and groundwater transport at Mt. Etna volcano (Sicily). *Geochim. Cosmochim. Acta* **64**, 1827–1841 (2000).
85. S. Rad, K. Rivé, C. J. Allegre, Weathering regime associated with subsurface circulation on volcanic islands. *Aquat. Geochem.* **17**, 221–241 (2011).
86. K. L. Ferrier, C. S. Riebe, W. Jesse Hahm, Testing for supply-limited and kinetic-limited chemical erosion in field measurements of regolith production and chemical depletion. *Geochem. Geophys. Geosyst.* **17**, 2270–2285 (2016).
87. D. Blackwell, "A summary of deep thermal data from the Cascade Range and analysis of the "rain curtain" effect" Oregon Department of Geology and Mineral Industries Open-File Report (1994), pp. 75–131.
88. J. Margat, J. Van der Gun, *Groundwater Around the World: A Geographic Synopsis* (Crc Press, 2013).
89. M. Safeeq, G. E. Grant, S. L. Lewis, M. G. Kramer, B. Staab, A hydrogeologic framework for characterizing summer streamflow sensitivity to climate warming in the Pacific Northwest, USA. *Hydrol. Earth Syst. Sci.* **18**, 3693–3710 (2014).
90. C. Tague, G. E. Grant, Groundwater dynamics mediate low-flow response to global warming in snow-dominated alpine regions. *Water Resour. Res.* **45**, W07421 (2009).
91. S. D. Willett, M. T. Brandon, On steady states in mountain belts. *Geology* **30**, 175–178 (2002).
92. Fasth, L. Karlstrom, Deep critical zone state shifts hydrology and well logs. HydroShare. https://doi.org/10.4211/hs.a042c5cb427b45279494b87dc305ed7d. Deposited 2 December 2024.
93. L. B. Ball *et al*., Surface geophysical data from Ollalie North springs, west-central Oregon. ScienceBase. https://doi.org/10.5066/P1KUJEIP. Deposited 2 December 2024.